AIAA JOURNAL
Vol. 37, No. 3, March 1999

Modeling and Validation of Induced Strain Actuation of Composite Coupled Plates

Chang-Ho Hong* and Inderjit Chopra†
University of Maryland, College Park, Maryland 20742

A consistent plate finite element model is formulated for coupled composite plates with induced strain actuation and validated with test data obtained from cantilevered isotropic and anisotropic plates. Actuators are modeled as additional plies fully integrated into substrate laminae, and the formulation is based on modified thin classical laminated-plate theory. The analysis is formulated for a generic anisotropic plate with a number of piezoactuators of arbitrary size, surface-bonded or embedded at arbitrary locations. Composite plates with extension-twist and bending-twist couplings were built and tested. Two rows of piezoceramic elements are surface mounted on both top and bottom surfaces near the root. Static tests are carried out using induced strain actuation, and mechanical loading and measured data are correlated with predictions for bending and twist distributions. For an extension-twist coupled plate, the agreement between predicted and measured induced twist due to extensional strain with piezoactuation is excellent. For the strongly bending-twist coupled composite plate, the predicted induced twist due to bending strain with piezoactuation agreed well in trends, but magnitudes were underpredicted by a maximum of 20% from measured values. For the weakly bending-twist coupled composite plate, the predicted induced-twist angle agreed extremely well with measured data. The modeling and validation results show the usability of the piezoactuation in the field of plate shape control.

Introduction

ADAPTIVE structures with embedded or surface-mounted strain-induced actuators are evolving in applications to various physical systems to actively control vibration, noise, aeroelastic stability, damping, shape, and stress distribution. Physical systems range from spacecraft, fixed-wing, and rotary-wing aircraft to automotive and other ground systems. One of the basic elements of adaptive structures is a thin composite plate with such distributed induced strain actuators as piezoceramic actuators. With tailored anisotropic plates, induced strain actuation can be used to control the extension, bending, and twisting of the structure.

The state-of-the-art on modeling of composite laminated plates, with induced strain actuation and systematic validation with test data, is limited. Most analyses assume piezoactuators as additional plies fully integrated with laminae of the substrate and use thin classical laminated-plate theory (CLPT) to develop formulations. Crawley and Lazarus[1] developed a simple Rayleigh–Ritz analysis of isotropic and anisotropic plates with induced strain actuation and validated it with test data they obtained by the testing of cantilevered isotropic and composite plates with piezoelectric actuators (surface-mounted entirely on both surfaces). Nonlinear piezoelectric constants (d_{31} and d_{32}) were measured experimentally and included in the analysis using an iterative procedure. Results demonstrated the validity of the model for some selected plate configurations as well as the potential of using induced strain actuation for shape control of elastic structures. Lee[2] also developed a thin laminated composite plate formulation with piezoelectric laminae using linear actuation characteristics. A limited validation study was carried out with data obtained from the testing of a thin composite plate actuated with piezoelectric polymer film (PVDF and PVF2). Wang and Rogers[3] applied classical laminated-plate theory to determine the equivalent force and moment induced by finite-length piezoactuators attached to a laminate. Using linear piezo characteristics, they showed that induced inplane forces and line moments along four edges of the actuator cause bending and extension of the plate. The refined composite plate theories with induced strain actuation were developed by Mitchell and Reddy[4] but were not substantiated with test data or results from other theories. Ha et al.[5] developed a linear finite element analysis of a laminated composite plate containing distributed piezoceramics. An eight-node three-dimensional composite brick element was incorporated into the analysis. Predicted induced deflections from surface-bonded piezoactuators were compared with test data from Ref. 1. The agreement was less than satisfactory, in particular for induced twist. Shah et al.[6] also developed a linear finite element analysis of laminated plates with piezoelectric plies. A nine-node isoparametric quadrilateral element was implemented in the analysis. No validation studies were carried out. Most of the existing analyses use linear piezoelectric characteristics and are not validated systematically with test data. The intent of this paper is to address these two important issues.

The present paper develops a consistent finite element laminated-plate analysis for a thin coupled composite plate with piezoelectric actuators placed at arbitrary locations. The formulation uses direct nonlinear free strain characteristics of actuators that are obtained by polynomial fitting to the test data. Systematic static tests are carried out on thin aluminum and coupled bending-twist and extension-twist graphite/epoxy plates with surface-mounted piezoceramics for part of the plate. Test data are used for validation of the analysis.

Analytical Modeling

The consistent plate model is formulated for the analysis of a laminated plate bonded with piezoceramic actuators. The assumptions made are as follows: 1) actuators and substrate are integrated as plies of a laminated plate, 2) consistent deformation exists in the actuators and substrate, and 3) laminate plate theory is adopted, but transverse shear deformation is allowed (the line originally normal to the midplane of the plate becomes inclined to the midplane after bending deflection). Assumptions 1 and 2 imply a perfect bonded condition between actuators and substrate. This is a generic thin-plate analysis for anisotropic plates with a number of actuators of arbitrary size, surface-bonded or embedded, and placed at arbitrary locations. Based on the preceding assumptions, the strains in the plate are

$$\varepsilon = \begin{Bmatrix} \varepsilon^0 \\ z\kappa \\ \gamma \end{Bmatrix} \tag{1}$$

Presented as Paper 97-1311 at the AIAA/ASME/ASCE/AHS/ASC 38th Structures, Structural Dynamics, and Materials Conference, Kissimmee, FL, April 7–10, 1997; received Aug. 26, 1997; revision received Nov. 15, 1998; accepted for publication Nov. 24, 1998.

*Visiting Professor, Department of Aerospace Engineering; currently Associate Professor, Department of Aerospace Engineering, Chungnam National University, Daejon 305-764, Republic of Korea.

†Alfred Gessow Rotorcraft Professor and Director Alfred Gessow Rotorcraft Center, Department of Aerospace Engineering. Fellow AIAA.

$$\boldsymbol{\varepsilon}^0 = \begin{Bmatrix} \varepsilon_x^0 \\ \varepsilon_y^0 \\ \gamma_{xy}^0 \end{Bmatrix}, \qquad \boldsymbol{\kappa} = \begin{Bmatrix} \kappa_x \\ \kappa_y \\ \kappa_{xy} \end{Bmatrix} = \begin{Bmatrix} \dfrac{\partial \theta_x}{\partial x} \\ \dfrac{\partial \theta_y}{\partial y} \\ \dfrac{\partial \theta_x}{\partial y} + \dfrac{\partial \theta_y}{\partial x} \end{Bmatrix} \tag{2}$$

$$\boldsymbol{\gamma} = \begin{Bmatrix} \theta_x - \dfrac{\partial w}{\partial x} \\ \theta_y - \dfrac{\partial w}{\partial y} \end{Bmatrix}$$

where ε_x^0, ε_y^0, and γ_{xy}^0 are midplane strains and θ_x and θ_y are plate rotation angles from z, the reference coordinate axis normal to the midplane of the plate before bending.

The constitutive relation for any ply of a laminated plate is

$$\boldsymbol{\sigma} = \boldsymbol{Q}(\boldsymbol{\varepsilon} - \boldsymbol{\Lambda}) \tag{3}$$

where

$$\boldsymbol{\sigma} = \begin{Bmatrix} \sigma_x \\ \sigma_y \\ \tau_{xy} \\ \tau_{xz} \\ \tau_{yz} \end{Bmatrix}, \qquad \boldsymbol{\Lambda} = \begin{Bmatrix} \Lambda_x \\ \Lambda_y \\ 0 \\ 0 \\ 0 \end{Bmatrix} \tag{4}$$

and $\boldsymbol{Q}$ is the transformed reduced stiffness matrix of the ply. Here the substrate is assumed to consist of anisotropic laminae, and the actuators are isotropic laminae. In the induced actuation strain vector $\boldsymbol{\Lambda}$ there is no shear strain component in it.

Finite Element Formulation

The total potential energy of the system is given by

$$\Pi = U - W \tag{5}$$

where U is the strain energy and W is the work done by the external forces. U can be expressed as

$$U = \frac{1}{2}\int_V \boldsymbol{\varepsilon}^T \boldsymbol{Q} \boldsymbol{\varepsilon}\, \mathrm{d}V - \int_V \boldsymbol{\varepsilon}^T \boldsymbol{Q} \boldsymbol{\Lambda}\, \mathrm{d}V \tag{6}$$

An eight-node plate element is used to model the laminated plate. The plate displacement vector $\boldsymbol{u}$ has five degrees of freedom and is given as

$$\boldsymbol{u} = \begin{Bmatrix} u \\ v \\ w \\ \theta_x \\ \theta_y \end{Bmatrix} \tag{7}$$

For the finite element discretization $\boldsymbol{u}$ is expressed using shape function matrix $\boldsymbol{\Phi}$ [Ref. 7] and nodal displacement vector $\boldsymbol{d}$ as

$$\boldsymbol{u} = \boldsymbol{\Phi} \boldsymbol{d} \tag{8}$$

The generalized strain-displacement relation for the plate-bending element allowing inplane displacements can be written as

$$\boldsymbol{\varepsilon} = \boldsymbol{B} \boldsymbol{u} \tag{9}$$

where $\boldsymbol{B}$ is the strain-displacement matrix and $\boldsymbol{B}_i$, $\boldsymbol{B}$ of the ith node, is given as

$$\boldsymbol{B}_i = \begin{bmatrix} \dfrac{\partial \phi_i}{\partial x} & 0 & \dfrac{\partial \phi_i}{\partial y} & 0 & 0 & 0 & 0 & 0 \\ 0 & \dfrac{\partial \phi_i}{\partial y} & \dfrac{\partial \phi_i}{\partial x} & 0 & 0 & 0 & 0 & 0 \\ 0 & 0 & 0 & 0 & 0 & 0 & -\dfrac{\partial \phi_i}{\partial y} & -\dfrac{\partial \phi_i}{\partial x} \\ 0 & 0 & 0 & \dfrac{\partial \phi_i}{\partial x} & 0 & \dfrac{\partial \phi_i}{\partial y} & 0 & \phi_i \\ 0 & 0 & 0 & 0 & \dfrac{\partial \phi_i}{\partial y} & \dfrac{\partial \phi_i}{\partial x} & \phi_i & 0 \end{bmatrix} \tag{10}$$

where ϕ_i is the shape function of the ith node.

A selectively reduced integration scheme is used to eliminate locking effects. Using the preceding equations and applying the principle of virtual work, the finite element formulation can be written as

$$\boldsymbol{K}^e \boldsymbol{d}^e = \boldsymbol{P}_\Lambda^e + \boldsymbol{F}^e \tag{11}$$

where $\boldsymbol{K}^e$, $\boldsymbol{P}_\Lambda^e$, and $\boldsymbol{F}^e$ are the element stiffness matrix, actuation load vector, and external load vector, respectively. These are expressed as

$$\begin{aligned} \boldsymbol{K}^e &= \int_V \boldsymbol{B}^T \boldsymbol{Q} \boldsymbol{B}\, \mathrm{d}V \\ \boldsymbol{P}^e &= \int_V \boldsymbol{B}^T \boldsymbol{Q} \boldsymbol{\Lambda}\, \mathrm{d}V \\ \boldsymbol{F}^e &= \int_S \boldsymbol{\Phi}^T \boldsymbol{f}\, \mathrm{d}S \end{aligned} \tag{12}$$

where $\boldsymbol{\Phi}$ is the shape function matrix[7] and $\boldsymbol{f}$ is the external applied nodal load vector.

Experiment

Free strain tests were carried out on piezoelements of size (25.4 × 50.8 × 0.254 mm) to determine strain at several voltages. Then a polynomial curve fitting was made to the test data (Fig. 1). In Fig. 1, the induced strains in each orthogonal direction were approximated by

$$\Lambda = 0.2643E + 0.00028E^2 \tag{13}$$

where E is the applied electric field, V/mm.

Aluminum and composite plates of rectangular size (393.7 × 152.4 mm) were manufactured. Graphite/epoxy plates with bending-twist and extension-twist coupling were built, each consisting of six plies. Table 1 shows the material properties of piezoceramic (Morgan–Matroc PZT-5H), aluminum, and graphite/epoxy (Hercules AS4/3501). Table 2 shows the layup of composite plates. To achieve a cantilevered condition, a part of plate length

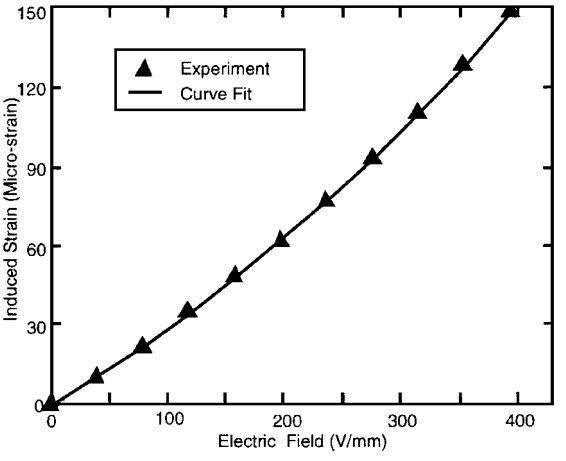

Fig. 1 Free-induced strain of piezoelement (PZT-5H). Experimental measurement and polynomial curve fitting.

Table 1 Material properties of piezoceramic (PZT-5H), aluminum, and graphite/epoxy (AS4)

Plates	Material properties
Piezoceramic (PZT-5H)	$E = 63.0$ GPa, $\nu = 0.3$
Aluminum	$E = 70.0$ GPa, $\nu = 0.3$
Graphite/epoxy (AS4)	$E_L = 143.0$ GPa, $E_T = 9.7$ GPa
	$G_{LT} = 6.0$ GPa, $\nu_{LT} = 0.42$

Table 2 Properties of aluminum and composite plates

Plates	Properties
Aluminum	$t = 0.76$ mm
Graphite/epoxy $[+45_3/-45_3]$	Extension-twist coupling, $t = 1.04$ mm
Graphite/epoxy $[+30_2/0]_s$	Bending-twist coupling, $t = 0.81$ mm
Graphite/epoxy $[0/\pm 45]_s$	Bending-twist coupling, $t = 0.79$ mm

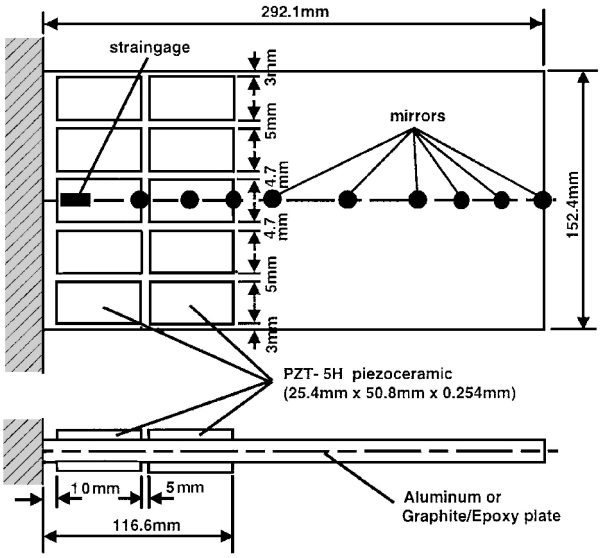

Fig. 2 Cantilevered plate with surface mounted piezoceramics.

(101.6 mm) is supported with thick aluminum bars, leaving an effective plate length of 292.1 mm. The 40% root end of the plate is surface-bonded with 10 equally spaced actuators ($25.4 \times 50.8 \times 0.254$ mm) on either surface.

Two rows of piezoceramic elements were bonded symmetrically on both the top and bottom surfaces of the aluminum and composite plates. The composite plates were sanded to expose fibers. The aluminum and composite plates acted directly as a common electrode for piezoceramic elements. The resistance of the composite plate was about 30 Ω, much higher than that of aluminum, but there was no measurable heat generation during the static tests. The cantilevered aluminum plate was tested first to verify its induced strain performance. In addition to piezoactuation, an external load of 40 g mass (0.392 N) was applied as a point-load at the tip of plate. Longitudinal and lateral slopes and twist with tip load and actuation were obtained, respectively. To avoid possible creep phenomena, the application of voltages to the desired level was done as quickly as possible. As expected, the creep behavior of piezoceramics was not noticeable under mechanical loading.

Slope angles were measured at discrete locations along the plate span using a laser-optic system: 60.8, 91, 116.6, 136, 178, 245, 268, and 292 mm from the root. Figure 2 shows the arrangement of the 10 actuator elements on each surface and also locations of mirrors. Bending actuation was applied to the aluminum and the bending-twist coupled plates. For the aluminum plate, longitudinal slopes were measured at midchord whereas lateral slopes were measured at the side edge. For bending-twist coupled plates both longitudinal slopes and twist angles were measured at midchord. For the extension-twist coupled plate, where actuation was in extension, only twist angles were measured. Test results shown in the figures are the averaged values from two specimens of each plate except the aluminum plate of which measurements were in excellent agreement with the results of the analysis. Specimens that gave unacceptable data were discarded. To take into account the hysteresis of piezoceramics (property of producing residual strains after removal of applied voltage), applications of electric voltages are repeated reversing the direction of electric potential. The measured results shown in the figures represent the absolute averaged values. For each plate results of finite element analysis due to tip loading were verified with measured values to validate the basic analysis. Then, similar tests were carried out with the piezoactuation, and data were used to validate modeling of composite plates with induced strain actuation.

Results and Discussion

For plate analysis, 198 rectangular finite elements (11×18) involving 3265 degrees of freedom are used (Fig. 3).

Figure 4 shows the longitudinal bending-slope distribution at midchord of an aluminum plate due to a mechanical load of 40 g at the tip. Both predicted results and measured data are presented. The correlation appears very good for this uncoupled plate. The piezoactuators are attached up to 40% of the plate length from the root resulting in a sudden change of slope distribution at the longitudinal station of 120 mm. This change can be attributed to the reduction of effective plate stiffness (absence of stiffness augmentation due to piezos) beyond this station. Figure 5 presents the longitudinal bending slope of the aluminum plate due to bending actuation with piezoceramics. Piezoceramic elements on the top and bottom surfaces are respectively excited by positive and negative potential of 100 V. The bending slope increases up to 40% in length, and then a slight reduction takes place beyond this length. Predictions agree extremely well with test data.

Figure 6 presents finite element results of longitudinal bending slopes of an aluminum plate due to piezo excitation at 100 V using linear and nonlinear piezoelectric constants for comparison purposes. The plot using curve-fit data in Fig. 6 is identical with the one by the finite element method (FEM) in Fig. 5. The values using

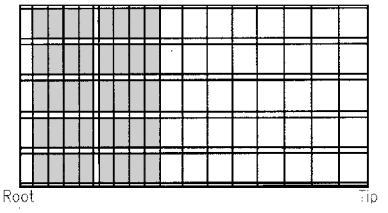

Fig. 3 Finite element modeling of the cantilever plate showing element distribution. Shaded areas represent mounted piezoceramics.

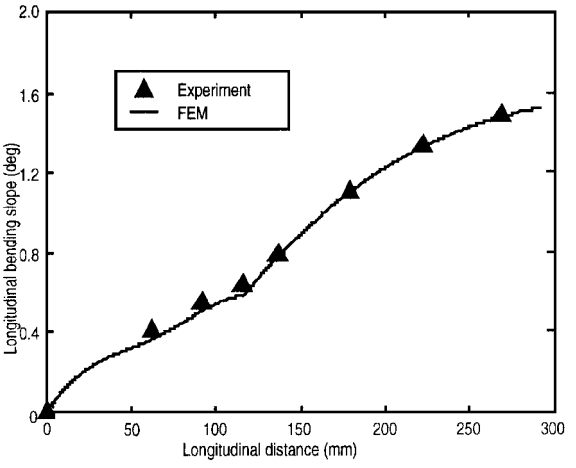

Fig. 4 Longitudinal bending slope at midchord of an aluminum plate due to a mechanical load of 40 g at the tip.

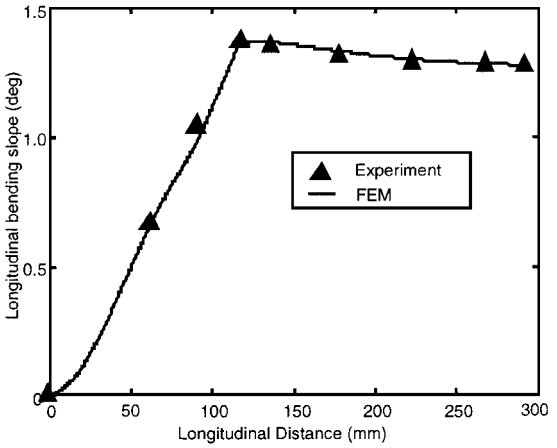

Fig. 5 Longitudinal bending slope at midchord of an aluminum plate due to piezobending excitation at 100 V (positive voltage to top piezos and negative voltage to bottom piezos).

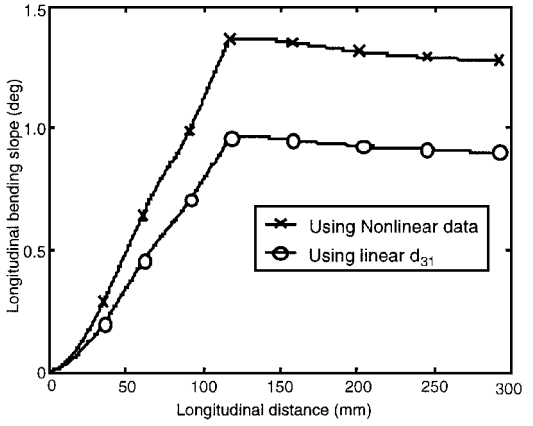

Fig. 6 Finite element results of longitudinal bending slopes at midchord of an aluminum plate due to piezoexcitation at 100 V using linear and nonlinear piezoelectric constants.

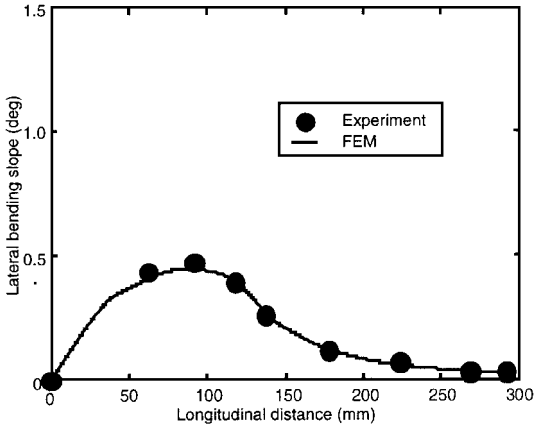

Fig. 7 Lateral-bending slope at side edge of an aluminum plate due to piezobending excitation at 100 V.

a nonlinear constant are 42% higher than those using a linear constant. The big differences between the two plots in Fig. 6 clearly show the importance of the nonlinear piezoelectric characteristics. The nonlinear characteristics of piezoceramic actuators are used as input data for the load vector and hence do not require an iterative procedure. This is a key difference from other analyses.[1]

Figure 7 presents the lateral bending-slope distribution at the side-edge for this aluminum plate. The lateral bending slope increases

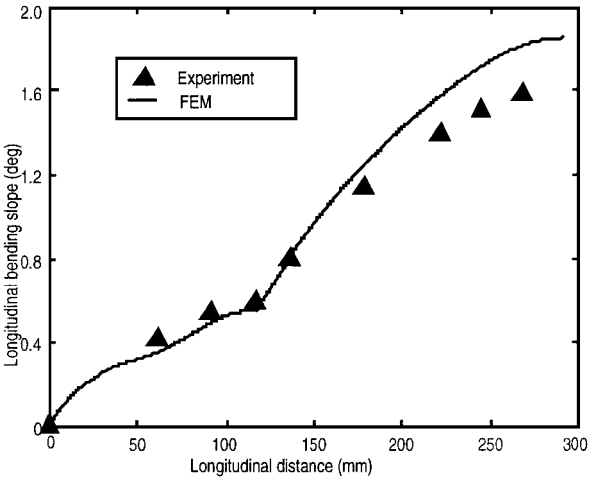

Fig. 8 Longitudinal bending slope at midchord of an extension-twist coupled [+45$_3$/−45$_3$] graphite/epoxy plate due to a mechanical load of 40 g at the tip.

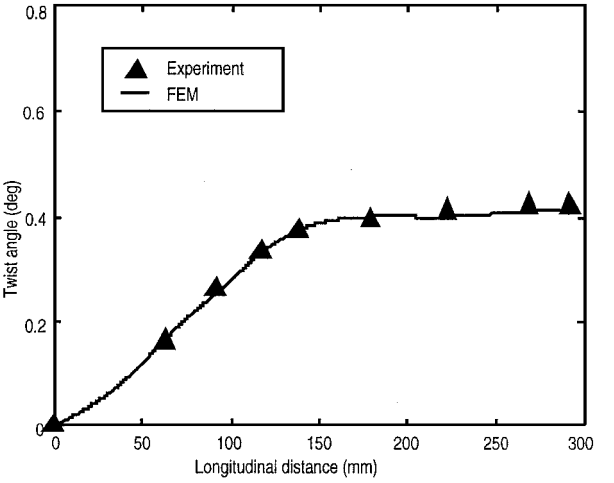

Fig. 9 Twist distribution at midchord of an extension-twist coupled [+45$_3$/−45$_3$] graphite/epoxy plate due to piezoexcitation at 100 V (same voltages to top and bottom piezos).

up to perhaps 40% in length and then gradually falls to a very small value at the tip. Again, the correlation between predicted and measured values is quite good.

Figures 8 and 9 present results for an antisymmetric layup graphite/epoxy plate. This causes an extension-twist coupling. An axial load, in addition to stretching, will also cause twisting of the plate, and the bending is uncoupled. Figure 8 shows longitudinal bending slopes due to a mechanical load of 40 g at the tip. The slope increases toward the tip, and again there is a sudden change at 40% in length. Predictions agree satisfactorily except near the tip where calculated values are higher than measured values by about 10%. The tendency of lower measured values than predictions is all common for coupled plates point-loaded mechanically at the tip, although for this antisymmetric layup plate the discrepancy is rather large. It may be due to the imperfect point-loading condition compared to the analytic method. Figure 9 presents the twist distribution for this plate due to axial actuation with piezos. For this setup, the same voltage of 100 V is applied to both top and bottom piezoceramics. Because of extension-twist coupling, a longitudinal strain will induce twisting of the plate. Predictions of twist agree extremely well with the test data. Because the axial strain stops at 40% length, there is almost no change of induced twist beyond 40% length.

Figures 10–13 present results for symmetric layup graphite/epoxy plates. This layup causes a bending-twist coupling. An induced bending actuation also will cause twisting of the plate, and the extension remains uncoupled. Figures 10 and 11 are for $[+30_2/0]_s$ plate, where bending-twist coupling is designed to be

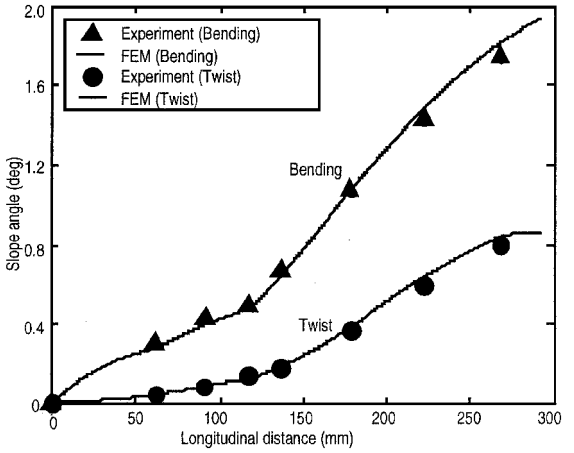

Fig. 10 Longitudinal bending and twist distribution at midchord of a bending-twist coupled $[+30_2/0]_s$ graphite/epoxy plate due to a mechanical load of 40 g at tip.

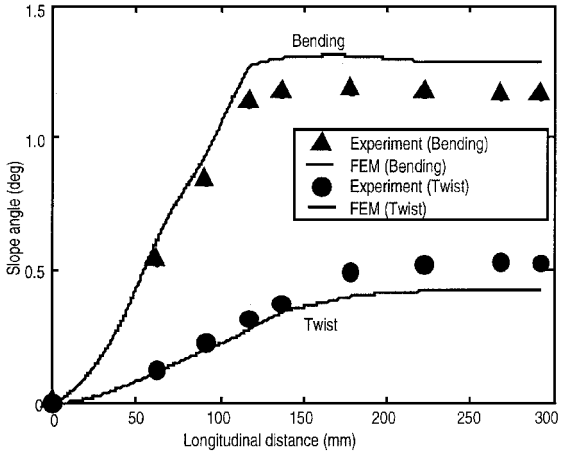

Fig. 11 Longitudinal bending and twist distribution at midchord of a bending-twist coupled $[+30_2/0]_s$ graphite/epoxy plate due to piezobending excitation at 100 V.

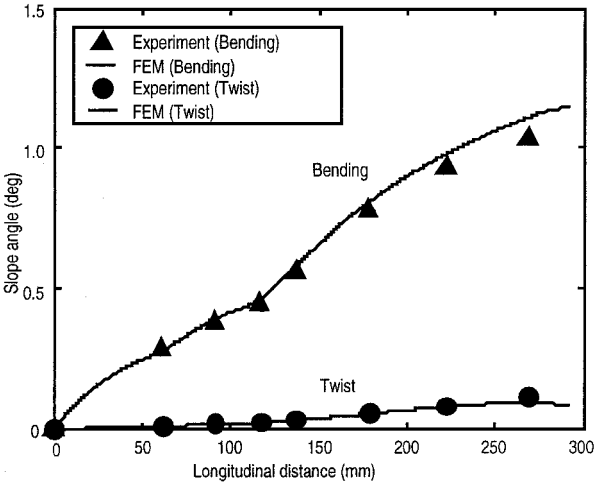

Fig. 12 Longitudinal bending and twist distribution at midchord of a bending-twist coupled $[0/\pm 45]_s$ graphite/epoxy plate due to a mechanical load of 40 g at the tip.

strong, whereas Figs. 12 and 13 are for $[0/\pm 45]_s$ plate, where bending-twist coupling is designed to be weak. Figure 10 shows the longitudinal bending and twist distributions for the strongly coupled plate due to a mechanical load of 40 g at the tip. Predictions for both bending slope and twist angle are very good. Figure 11 presents the longitudinal bending slopes and twist distributions for this plate due to induced bending actuation. For this case, opposite potential is applied to the top and bottom piezoceramic actuators. The calculated

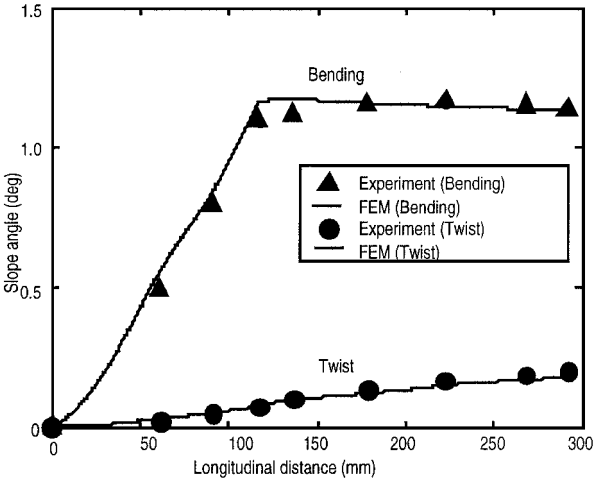

Fig. 13 Longitudinal bending and twist distribution at midchord of a bending-twist coupled $[0/\pm 45]_s$ graphite/epoxy plate due to piezobending excitation at 100 V.

longitudinal bending slope is somewhat overpredicted from measured values, more so toward the tip where deviations are less then 11%. Predictions for twist angles are good up to around 50% length but, beyond this, are lower than measured values by as much as 20%. Overall predictions are satisfactory, and trends are predicted well. These large discrepancies may be due to the strong coupling effect and also can be seen in Ref. 1.

Figure 12 shows the longitudinal bending and twist distributions for the weakly coupled plate due to a mechanical tip load of 40 g. Predictions for the bending slopes are very good except near the tip. Predictions for the twist angle agree very well with test data. Figure 13 shows longitudinal bending and twist distributions for this plate due to induced bending actuation with an excitation of 100 V. Predictions for both bending slope and twist angle are quite good.

Conclusions

Analysis of thin-coupled composite plates with induced strain actuation due to piezoceramics is developed using plate finite element discretization. Aluminum and bending-twist and extension-twist graphite/epoxy plates were built with surface-mounted piezoceramics on both top and bottom surfaces for part of the plate. Measured slopes and twist distributions were correlated with predictions. For an aluminum plate, the predicted longitudinal slopes due to an induced field of 100 V agreed extremely well with test data. For an extension-twist coupled plate the agreement between predicted and measured induced twist due to extensional strain with piezoactuation was excellent. For the strongly bending-twist coupled composite plate, the predicted induced twist due to bending strain with piezoactuation agreed well in trends, but magnitudes were underpredicted by a maximum of 20% from measured values. For the weakly bending-twist coupled composite plate the predicted induced-twist angle agreed extremely well with measured data. From these results the following conclusions are drawn:

1) The present finite element modeling is capable of predicting the response of the composite coupling plates with piezoelectric actuation.

2) The use of nonlinear piezoelectric constants is verified by good agreements between test and predicted data. Also the use of an iterative procedure as suggested in Ref. 1 for the calculation of the load vector is found to be unnecessary.

3) For the strongly bending-twist coupled plate, the twist to bending-coupling ratio of the test is much higher than that of the prediction. This interesting behavior requires further validation study.

4) Finally, the modeling and validation results show the usability of the piezoelectric actuation in the field of plate shape control.

Acknowledgments

This research work was supported by the U.S. Army Research Office under Multidisciplinary University Research Initiative Contract DAAH-04-96-10334 with Technical Monitors Gary Anderson and Tom Doligaski.

References

[1]Crawley, E. F., and Lazarus, K. B., "Induced Strain Actuation of Isotropic and Anisotropic Plates," *AIAA Journal*, Vol. 29, No. 6, 1991, pp. 944–951.

[2]Lee, C. K., "Piezoelectric Laminates: Theory and Experiments for Distributed Sensors and Actuators," *Intelligent Structural Systems*, edited by H. S. Tzou, and G. L. Anderson, Kluwer Academic, Norwell, MA, 1992, pp. 75–168.

[3]Wang, B. T., and Rogers, C. A., "Laminate Plate Theory for Spatially Distributed Induced Strain Actuators," *Journal of Composite Materials*, Vol. 25, No. 4, 1991, pp. 433–452.

[4]Mitchell, J. A., and Reddy, J. N., "A Refined Hybrid Plate Theory for Composite Laminates of Piezoelectric Laminae," *International Journal of Solids and Structures*, Vol. 32, No. 16, 1995, pp. 2345–2367.

[5]Ha, S. K., Keilers, C., and Chang, F. K., "Finite Element Analysis of Composite Structures Containing Distributed Piezoelectric Sensors and Actuators," *AIAA Journal*, Vol. 30, No. 3, 1992, pp. 772–780.

[6]Shah, D. K., Chan, W. S., and Joshi, S. P., "Finite Element Analysis of Plates with Piezoelectric Layers," *Proceeding of the AIAA/ASME/ASCE/AHS/ASC 34th Structures, Structural Dynamics, and Materials Conference* (La Jolla, CA), AIAA, Washington, DC, 1993, pp. 3189–3197 (AIAA Paper 93-1678).

[7]Hinton, E., and Owen, D. R. J., *Finite Element Programming*, Academic, London, 1979.

A. M. Waas
Associate Editor